SCIENCE CHINA Materials

ARTICLES

mater.scichina.com link.springer.com

Published online 20 November 2015 | doi: 10.1007/s40843-015-0100-z
Sci China Mater 2015, 58: 867–876

Photocatalytic water oxidation by layered Co/*h*-BCN hybrids

Mingwen Zhang, Zhishan Luo, Min Zhou, Caijin Huang and Xinchen Wang*

A hexagonal boron carbon nitride (*h*-BCN) semiconductor was applied to intercalate cobalt ions to catalyze oxygen evolution reaction (OER) with light illumination, without using noble metals. The *h*-BCN with high specific surface area showed a strong chemical affinity towards metal ions due to the "lop-sided" densities characteristic of ionic B–N bonding, enabling the creation of metal/*h*-BCN hybrid layered structures with unique properties. As exemplified here by Co/*h*-BCN for water oxidation catalysis, after intercalating cobalt ions in the *h*-BCN host, the photocatalytic activity of the resultant layered hybrid is optimized due to their synergic catalysis that promotes charge separation and lowers reaction barriers. This finding promises a new nobel-metal-free nanocompsite using cost-acceptable and earth-abundant sustances for photocatalytic OER, and enables the facile design of duel catalytic cascades by merging transition metal catalysis with *h*-BCN (photo)catalysis for energy and sustainability.

INTRODUCTION

Solar irradiation provides a clean and unlimited energy resource to address energy and environmental issues [1–4]. Photocatalytic water splitting achieved on semiconductor diodes is facile and sustainable to capture, convert and store solar photons in a chemical fashion. Since the discovery of the Honda–Fujishima effect in 1972, one of the central challenges is still related to the search for stable, efficient, and earth-abundant photocatalysts, in particular the ones with robust water oxidation activity [5,6]. The water oxidation half reaction is the crucial step towards solar fuel conversion using water as feedstock [7,8], which not only requires an efficient pathway to bridge the one-electron photon capture process with the four-electron oxygen evolution reaction (OER), but also suffers from large kinetic barriers. The development of new semiconductors and kinetic promoters is therefore actively pursued nowadays, to liberate oxygen from water while releasing electrons and protons for fuel generations such as H_2 production and CO_2 reduction [9,10].

The search for new materials has progressed from metal-based photocatalysts to elemental semiconductors (C, Si, P, S, B) [11–15] and recently to metal-free binary materials and polymers, such as carbon nitride [16], boron carbide [17] and conjugated semiconductors [18–20]. These researches indicate that photon absorbing materials can be constituted by using lightweight elements such as carbon, nitrogen, and boron, opening up new opportunities for the selection of innovative and intriguing materials for artificial photosynthesis. It is of particular interest that some of these elements themselves (graphene [21], silicone [22]) or their combinations (*h*-BN, g-C_3N_4) [23] can form layered structures with reduced thickness comparable to charge-diffusion distance, and thus if a semiconducting electronic structure was imparted in these materials, the fast separation of light-induced charge carrier would significantly benefit surface photoredox process that relied on the excitation and separation of electron-hole pairs and their subsequent participation in surface chemical reactions [24–26]. An interesting case of such a layered material is ternary *h*-BCN with tuneable band gap energies between graphene (zero bandgap) and *h*-BN (bandgap = 5.6 eV) [27], which have the same atomic structure and share many similar properties. The hybridized phases of the two two-dimensional (2D) materials by atomic mixture of B, N, and C with broad composition ranges to create various layered semiconducting structures would produce new material functions complementary to graphene and *h*-BN, enabling a wide variety of electronic structures, applications and properties [28–30]. Such an emerging family of chemically inert and mechanically strong 2D materials practically allows the bandgap-engineered applications in heterogeneous photocatalysis by creating a medium-gap ternary semiconductor, in which the band gap, redox energy levels, p/n-type properties and surface acid-base chemistry can in principle be modulated by rational design and synthesis [31,32].

State Key Laboratory of Photocatalysis on Energy and Environment, College of Chemistry, Fuzhou University, Fuzhou 350002, China
* Corresponding author (email: xcwang@fzu.edu.cn)

Especially, theoretical and experimental investigations have indicated that visible light absorption and emission with tuneable wavelength can be achieved by controlling the carbon content in (B, N) rich BCN nanostructures, which then can be considered as metal-free light energy converters [33–35]. However, the study on this family of ternary photocatalysts is rather rare, although such materials fulfil basic requirements of photocatalysts, including being stable, visible-light responsive, and inexpensive. Importantly, it permits an ample choice of chemical/physical protocols to engineer surface and bulk structure of *h*-BCN to strengthen material functions and even to produce new properties distinct from graphene and *h*-BN.

Indeed, surface/interface engineering with metal ions are encouraged since BCN-based materials feature the "lop-sided" densities characteristic of ionic B–N bonding, and the polyelectronic nitride can transfer more electron density to metal ions [36,37]. They are thus effective for the adsorption of metal ions, chemically, as highlighted here by surface engineering via cobalt ions (Scheme 1). Such strong chemical interaction between Co ions and the *h*-BCN matrix provides the possibility of the migration of photo-induced holes from *h*-BCN to surface-bonded cobalt species. Thus, the holes with a measured oxidative potential of 1.59 V (*vs.* NHE at pH 7) at the top of the valance band can react with water on the cobalt active sites to produce oxygen, instead of the accumulation of the holes on *h*-BCN. The later always causes charge buildup that leads to the oxidization of *h*-BCN by the holes [16].

As our continuous effort to develop sustainable photochemical systems for OER, herein we have applied layered *h*-BCN semiconductor to cooperate with cobalt catalysts to achieve water oxidation reaction with light irradiation. The *h*-BCN samples were synthesized by a pyrolysis method coupled with a gas-phase nitridation under flowing ammonia gas at high temperatures. The obtained yellow *h*-BCN materials feature high specific surface area (284 $m^2 g^{-1}$) and porous structure even when the thermal treatment is as high as 1200°C, being valuable host materials for surface modification and engineering with catalytically, magnetically, and optically active species, for example cobalt catalysts as proposed here. The surface cobalt/*h*-BCN junctions thus fabricated can photocatalyze water oxidation reaction, without the requirement of noble metal catalysts, like RuO_2 or Ir_2O_3.

RESULTS AND DISCUSSION

First, we synthesized the *h*-BCN sample and performed characterizations on its crystal, chemical and surface structures (see Experimental Section). The crystal structure was examined by X-ray diffraction (XRD) and high-resolution transmission electron microscopy (HRTEM). The XRD pattern in Fig. 1a shows two main peaks at 25.8° and 42.7°, attributable to the (002) and (100) lattice planes

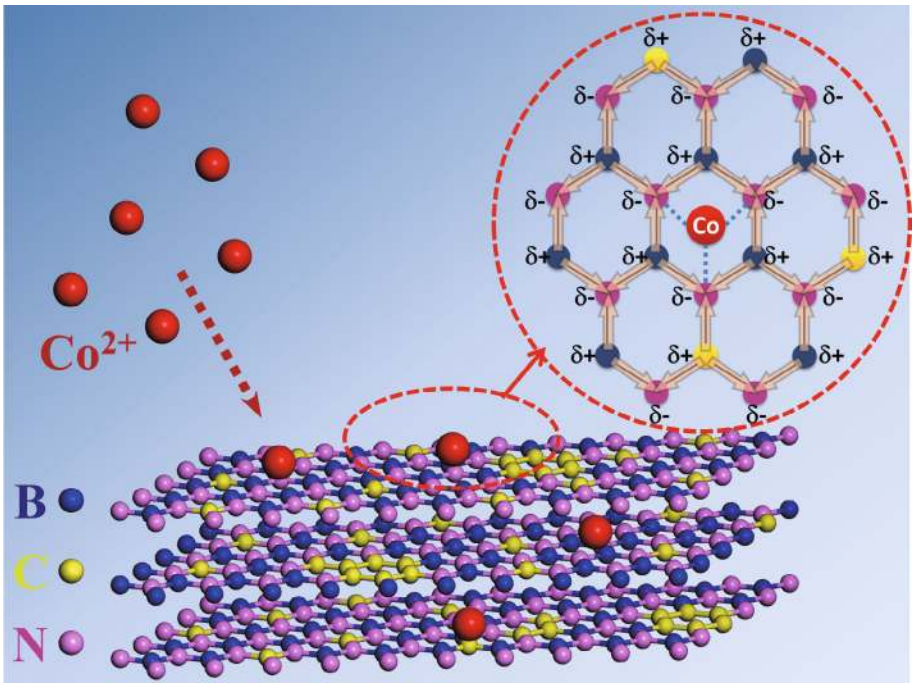

Scheme 1 The synthetic process of Co/*h*-BCN via chemical adsorption.

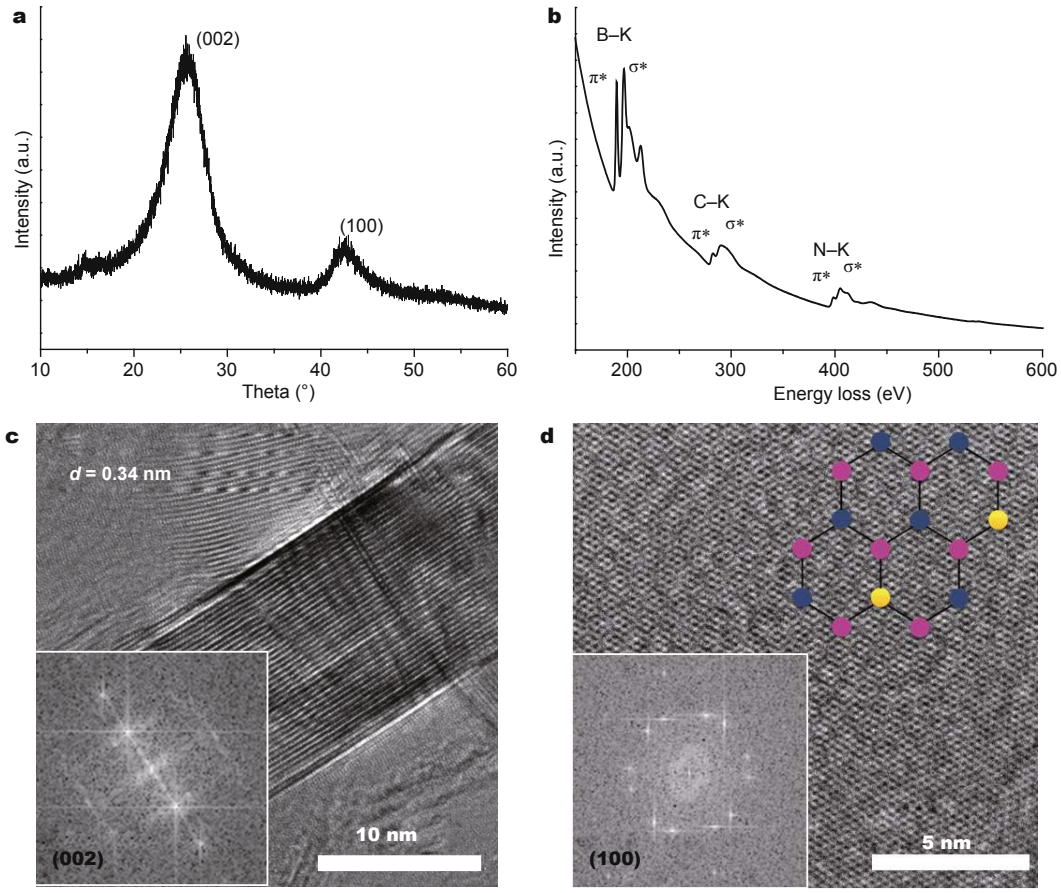

Figure 1 The powder XRD pattern (a), EELS spectrum (b) of *h*-BCN sample. HRTEM images of the edge (c) and the center (d) region of *h*-BCN. The insets are the fast Fourier transform pattern of the corresponding image.

in the graphite-like crystal structure, respectively [29]. The HRTEM image in Fig. 1c focusing on the edge region of *h*-BCN highlights the interlayer lattice fringes of 0.34 nm within the layered *h*-BCN, whereas Fig. 1d displays the atomic arrangements of unit cells in *h*-BCN. Fast Fourier transform (FFT) patterns in the inset revealed the (002) and (100) crystal planes for Figs 1c and 1d, respectively. Electron energy loss spectroscopy (EELS) in Fig. 1b reveals that the K-edge absorptions of B, C, and N atoms exhibit the sharp peaks followed by wider bands corresponding to the 1s-p* and 1s-s* transitions, respectively [29]. This is a clear sp^2-hybridization characteristic, indicating that the carbon atoms are in the same sp^2-hybridized state as their BN hosts.

Fig. S1 is the Fourier transform infrared (FTIR) spectrum of the sample, showing two strong peaks at 1400 and 790 cm^{-1} that are assigned to characteristic absorption bands of B–N bond [35]. The vibrations of the C-related group were all overlapped by that of B–N. The existence of C-related bonds was observed in the C 1s X-ray photoelectron spectroscopy (XPS) spectrum (Fig. S2). Raman signal for the *h*-BCN sample is not observed (Fig. S3), due to the structural distortion induced by the C substitution in layered *h*-BN, instead of a phase-separated structure made of C domains and BN [28]. This however indicates the doping of carbon in the *h*-BN crystal narrows the band gap by substitution of B with C, by which the hybridization of B 2p with C 2p orbitals also widens the density states of the conduction band that facilitates electron migration, being promising for photoredox catalysis. These are supported by the characterizations on the band structure and Nyquist plots of electrochemical impedance spectroscopy of the *h*-BCN electrodes (Figs 2 and S10a).

The first test of pristine *h*-BCN for water oxidation revealed a moderate photocatalytic activity with an oxygen evolution rate of 1.2 mmol h^{-1} only. The selectivity of light-induced holes (~17%) for converting water to O_2 is much lower than that toward the self-oxidation of

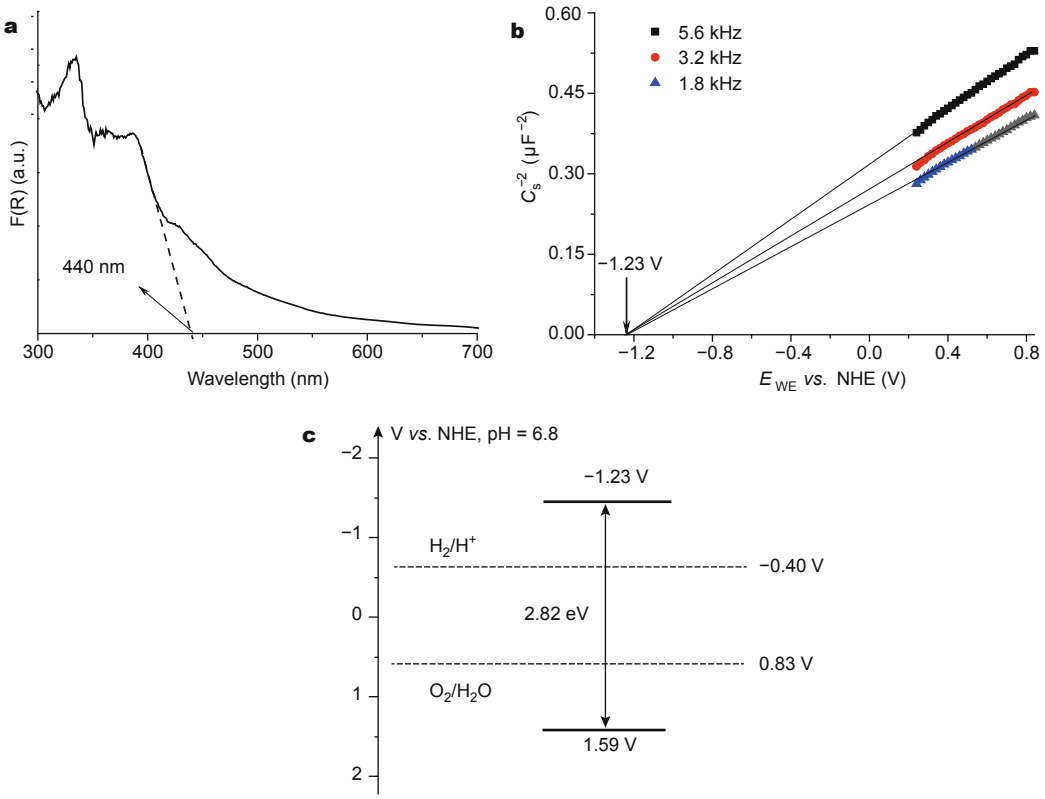

Figure 2 The band structure of *h*-BCN. (a) UV-vis DRS spectrum. (b) The determination of the conduction band minimum (CBM) of *h*-BCN by Mott-Schottky method. (c) The determined band structure with respect to normal hydrogen electrode (NHE).

h-BCN. This speaks for the fact that the pristine *h*-BCN is photocorroded due to the surface charge built-up without kinetic controls, because the N^{3-} anions in the nanostructured *h*-BCN are more susceptible to be oxidized than water by the light-generated holes. It is therefore necessary to make additional surface kinetic controls by rational decoration of oxidative co-factors on the *h*-BCN surface, which results in quick separation and migration of light-generated holes from the bulk to the active sites to oxidize water while still stabilizing the surface defective nitrogen sites by binding with the metal ions as the oxidative co-factors [38,39]. Here we first select cobalt ions because cobalt species have re-emerged as efficient redox co-catalysts in photocatalysis and photoelectrocatalysis [38–40], albeit the detailed physical insights on the working mechanism in terms of reactive structure of cobalt in molecular level are still under investigations. Considering this, together with the unique adsorption capacity of *h*-BCN towards metal ions, it is desired to construct surface metal/semiconductor junction between cobalt and *h*-BCN.

The chemical affinity of the *h*-BCN sample for binding Co^{2+} in water was therefore analyzed. Results show that the sample adsorbs cobalt ions at a maximum adsorption capability of ca. 22 mg g^{-1} with respect to *h*-BCN, corresponding to 2.2 wt.% Co. After a multiple washing the Co/*h*-BCN sample with water, the inductively coupled plasma (ICP) analysis results suggest that 99.8 % cobalt elements are remained in the sample, which indicates that cobalt ions are uniformly distributed and firmly anchored on the surface of *h*-BCN. This can be reflected in part by the elemental mapping analysis of the hybrid, which records the uniform distribution of the B, C, N and Co elements on the Co/*h*-BCN sample (Fig. 3), revealing the uniform dispersion of Co ions on the *h*-BCN host, same as the pristine counterparts (Fig. S4). However, we cannot find any solid-state cobalt species in the magnified TEM image in Fig. S5 [38]. This reveals that the cobalt species do not exist in the form of particles, but atomically dispersing on the N-rich matrix. XPS studies provide detailed information on the chemical state of Co species. As seen in Fig. S6, the Co 2p spectra consists of two high-resolution peaks at 782.0 and 797.4 eV, respectively, corresponding to Co(II) and Co(III) [41]. The satellite peak at 788.1 eV is a characteristic feature of Co^{2+} ions. The binding energy of Co(II) is less in value than that

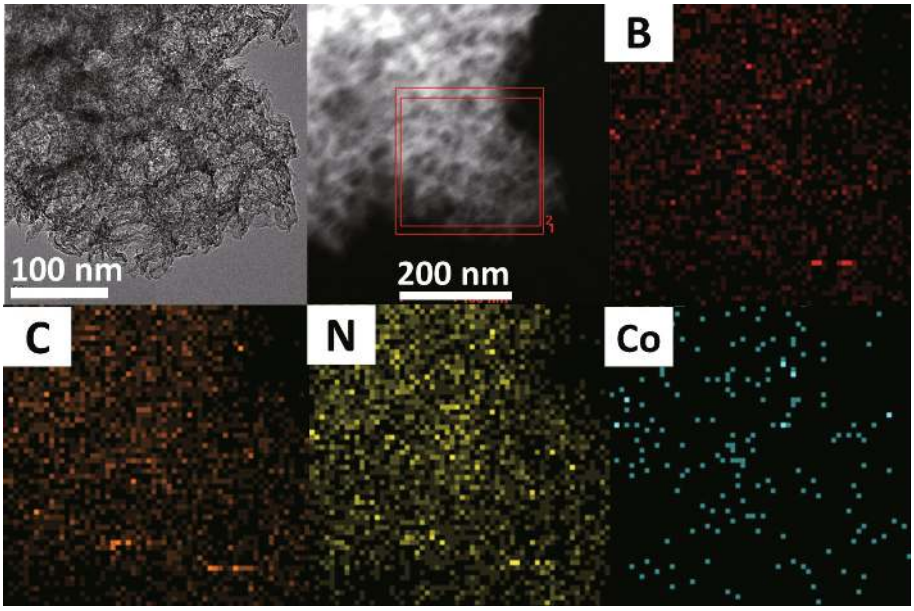

Figure 3 Typical TEM image of 0.7 wt.% Co/*h*-BCN with the elemental mapping of B, C, N and Co of the enlargement of the selected area.

of 782.8 eV present in the pure $Co(NO_3)_2$, indicative of a strong chemical interaction (electron coupling) between the Co and the *h*-BCN matrix [42]. This result confirms that the Co ions are stabilized by the *h*-BCN matrix and charges are able to transfer between them. The XRD patterns and FTIR spectra (Figs S7 and S8) of Co/*h*-BCN are identical to those for *h*-BCN. These observations indicate that the loading of Co species does not change the bulk structure of *h*-BCN and its core chemical skeleton, which promises the combination of cobalt catalysis with *h*-BCN photocatalysis to establish dual catalysis for targeted applications.

In the next set of experiments, we performed optical, electron paramagnetic resonance (EPR) and electrochemical characterizations of the Co/*h*-BCN layered hybrids. As shown in the UV-vis diffuse reflectance spectra (DRS) (Fig. 4a), the optical features of the *h*-BCN before and after loading with the Co species were analyzed. All samples display the long absorption tails, which again indicates the presence of intra-band impurity transitions potentially located at the surface. As we know, the 400–800 nm spectrum of $Co(NO_3)_2{\cdot}6H_2O$ in the solid state exhibits one main band at ~524 nm, which is assigned to the 4T1g → 4T1g (P) d-d transition [43]. This transition band is also present in Co/*h*-BCN, as indicated by the increase of the absorbance in DRS spectra of Co/*h*-BCN over *h*-BCN. In Fig. 4b, the strong photoluminescence (PL) emission peak is observed for the *h*-BCN sample, due to the radiative recombination of light-stimulated charge carriers, however the remarkable quenching of the PL peak was observed after the modification of the cobalt due to the localization of electrons in conduction band side (B 2p and C 2p) and holes in the valance band side (N 2p-*x*-*y*) linked to cobalt species via the lone pair electron in N 2p-*z*. Evidently, the binding of the cobalt promotes charge separation, particularly by the fast transfer of hole to material interface/surface via the Co-N linkages. In this regards, the fast charge release was achieved, which was beneficial for oxidation reaction. Such a spatial redistribution of charge carriers was also reflected by EPR analysis of the *h*-BCN and Co/*h*-BCN samples. In Fig. 4c, an asymmetric signal line centering at g = 2.0034 is observed for *h*-BCN and Co/*h*-BCN samples, indicating the generation of unpaired electrons on the conduction band containing C 2p orbitals [44]. The Lorentzian line can be enhanced after loading the Co species on *h*-BCN, due to the redistribution and the stabilization of the conjugated electron system (Fig. S9). This once again illustrates the tight interaction between Co ions and *h*-BCN, which optimizes the surface structure of the layered hybrids for charge separation.

The electrochemical measurements were performed to assess the effect of Co species on current-potential characteristics. As shown in Fig. 4d, the polarization curve (*I*-*V*) of *h*-BCN shows catalytically inert characteristics for water oxidation reaction even at large bias of ~1.7 V *vs.* RHE. By contrast, when the ITO electrode was coated with Co/*h*-BCN, a much greater current and earlier onset of catalytic current as compared to *h*-BCN was observed. This result

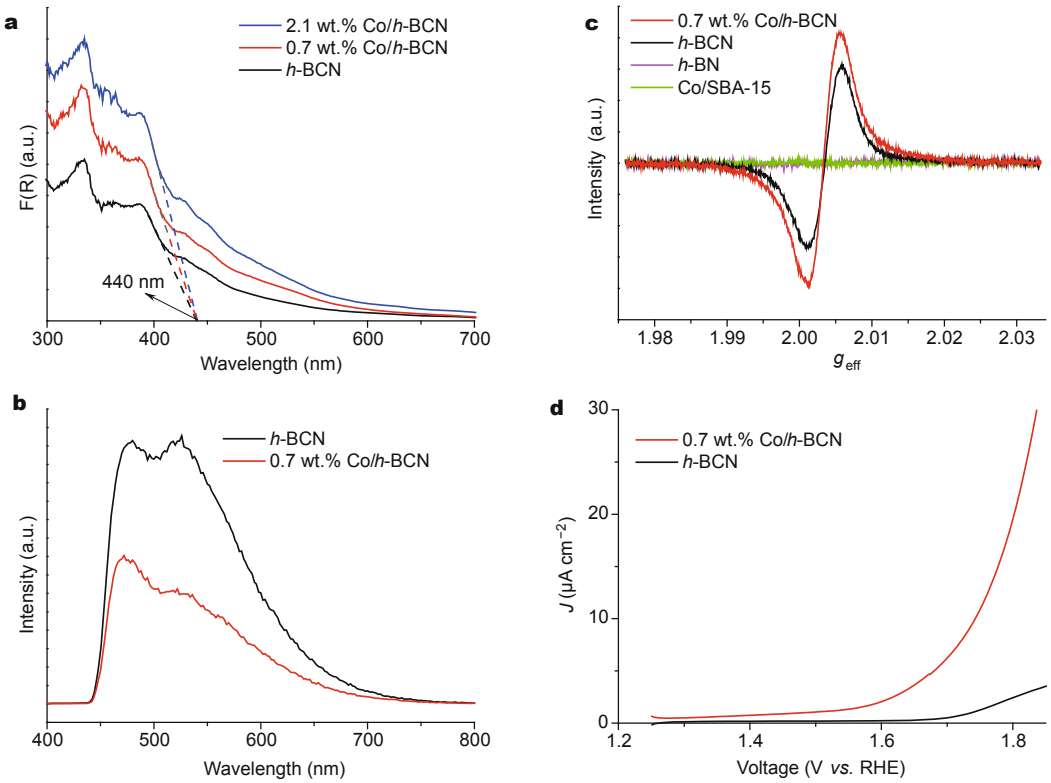

Figure 4 UV-vis DRS spectra (a), PL emission spectra (excitation wavelength is 380 nm) (b), EPR spectra in dark (c) and polarization curves in dark (d).

indicates that the chemical coupling and concomitant electron's redistribution between Co species and *h*-BCN can provide a resistance-less path for fast charge transfer through Co/*h*-BCN interface (Fig. S10). In addition, the Co species own an appropriate co-catalytic activity to lower overpotentials for water oxidation and consequently accelerate the electrocatalytic kinetics on the surface of the ternary *h*-BCN.

The water oxidation performance of Co/*h*-BCN samples under light irradiation was examined in a powder photocatalytic system. The loading of cobalt ion as an oxygen evolution cocatalyst can significantly increase the oxygen evolution rate to 10 mmol h^{-1}. In addition, the self-oxidation of nitride ions in the *h*-BCN matrix is suppressed. This result strongly suggests that the adsorbed Co species exhibit the functionality as effective O_2 evolution sites that capture photogenerated holes migrated from *h*-BCN matrix. A volcano-type curve of O_2 evolution activity depending on the amount of Co ions was observed, and the maximum oxygen evolution rate appeared for 0.7 wt.% Co/*h*-BCN (Fig. S11). An excessive amount of Co modifier leads to a decrease in the water oxidation activity, which could be ascribed to the light shielding effect [45–47]. Fig. 5 shows the detailed time course of O_2 evolution on the Co/*h*-BCN samples under both UV-vis and visible ($\lambda > 420$ nm) light irradiation. No gas evolution took place in the dark, and the reaction began with the onset of irradiation. The gradual decrease in the O_2 evolution rates was due to the reduced Ag^+ concentration and the photodeposition of Ag, which blocked the surface of the photocatalyst and shielded the incident light (Fig. S12).

The cocatalytic properties of the other Co complexes were also evaluated, and the results are shown in Table 1. A high oxygen evolution rate could be achieved by loading simple cobalt salts, such as $Co(NO_3)_2$ and $Co(COOH)_2$. As references, the Co species with electro-neutrality (cobaltocene, $(\eta5\text{-}C_5H_5)_2Co$) and electro-negativity (Co-bearing polyoxometalate, $[Co_4(H_2O)_2(PW_9O_{34})_2]^{10-}$) show a relatively minor effect on the water oxidation reaction. Compared with the electro-positive Co ions, these electro-neutral and electro-negative Co species are incompatible to charge with *h*-BCN matrix, resulting in sluggish reaction kinetics.

To underline the importance of the Co ions for water

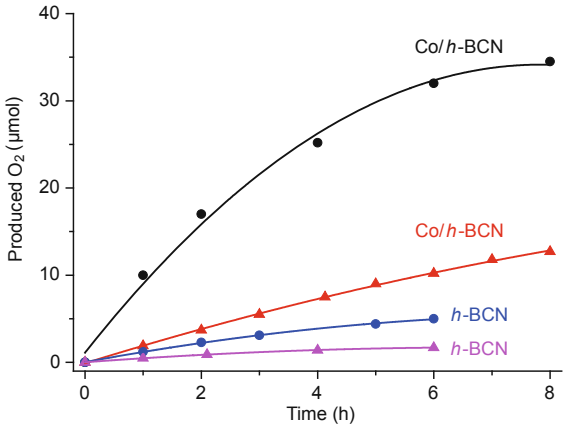

Figure 5 Time course of O_2 production for *h*-BCN and 0.7 wt.% Co/*h*-BCN under visible (λ > 420 nm, ▲) and UV–vis irradiation (λ > 300 nm, ●).

oxidation, we also investigated the behaviors of the other transition-metal ions (Cu^{2+}, Fe^{3+}, Mn^{2+}, Ni^{2+}, Cr^{3+}) as water oxidation cocatalysts. As shown in Table S1, the addition of Cu^{2+} and Fe^{3+} slightly enhanced the water oxidation performance, while Mn^{2+}, Ni^{2+} and Cr^{3+} had no effect on water oxidation rate. This reveals the unique properties of cobalt species in accelerating the water oxidation reaction. Nevertheless, these transition-metal ions can improve the selectivity of O_2 production, in comparison with *h*-BCN. This result reveals that the adsorption of metal ions could facilitate the holes migration from *h*-BCN to metal species, indicating chemical interactions between the metal ions and *h*-BCN networks. The integration of metal ions on nanostructured *h*-BCN therefore promises the development of a large number of sustainable catalysts with duel catalytic functions by merging transition metal catalysis with *h*-BCN (photo) catalysis, as also demonstrated by our case study of Fe/*h*-BCN for selective oxidation of benzene to phenol where Fenton catalysis has been promoted by *h*-BCN photocatalysis.

CONCLUSIONS

In summary, noble-metal-free photocatalysts and co-catalysts have been integrated for photocatalytic water oxidation by utilizing ternary *h*-BCN semiconductors and cobalt catalysts. The binding of cobalt ions on *h*-BCN matrix indeed promotes the separation and migration of light-driven holes, decreases the overpotentials for water oxidation, and consequently enhances the water oxidation activity. The results put a step towards artificial photosynthesis where the lightweight B, C, and N elements and inexpensive cobalt ions can be constructed as sustainable 2D semiconductor nanohybrids for addressing energy and environmental issues by photoredox catalysis. It is the high thermal and mechanical stabilities of *h*-BCN together with its high surface area and ease surface modifications that allow for the innovative and rational design of new heterogeneous (photo)catalysts for green synthesis, but also as 2D functional semiconductors for future electronic and (opto) electronic devices [48,49].

EXPERIMENTAL SECTION

Synthesis of *h*-BCN solids

Typically, boron oxide (2 g), urea (4 g) and glucose (0.6 g) were grinded fully with an agate mortar. After that, the mixed precursor was put into a horizontal tube furnace and heated at 1473 K for 5 h under a flow of ammonia (200 mL min^{-1}) at a heating rate of 5°C min^{-1}. Then, 250 mg powders were dispersed and washed in water (5 mL), with ultrasonic treatment. After rotary evaporation, the sample was placed in an alumina crucible to dry at 573 K for 1 h in air. The as-obtained final powder was donated as *h*-BCN.

Synthesis of *h*-BN solids

Typically, boron oxide (2 g) and urea (4 g) were grinded fully with an agate mortar. After that, the mixed precursor was put into a horizontal tube furnace and heated at 1473 K for 5 h under a flow of ammonia (200 mL min^{-1})

Table 1 Effects of different cobalt compounds as cocatalysts to promote O_2 evolution rate of *h*-BCN under light irradiation (λ >300 nm)

Entry	Photocatalyst	Cocatalyst	Amount of cocatalyst (wt.%)	O_2 evolution rate (mmol h^{-1})
1	*h*-BCN	–	–	1.2
2	*h*-BCN	$Co(NO_3)_2$	0.7	10.0
3	*h*-BCN	$[Co_4(H_2O)_2(PW_9O_{34})_2]^{10-}$	0.7	2.6
4	*h*-BCN	$Co(COOH)_2$	0.7	10.0
5	*h*-BCN	$Co(SO_4)_2$	0.7	6.9
6	*h*-BCN	$(\eta5\text{-}C_5H_5)_2Co$	0.7	1.5

at a heating rate of 5°C min^{-1}. The as-obtained powder was donated as *h*-BN.

Synthesis of Co/*h*-BCN

The as-prepared *h*-BCN sample was previously dispersed in water (5 mL). Then, different amount of $Co(NO_3)_2$ aqueous solution was added. After adsorbing for 0.5 h, the powders were washed by water for several times to remove the unadsorbed ions and dried at 80°C for characterization.

Characterization

XRD measurements were performed on a Bruker D8 Advance diffractometer with CuKα1 radiation (λ = 1.5406 Å). EELS investigation were carried out on a JEOL JEM-ARM200F microscope. TEM was operated by Tecnai20 FEG microscope and Titan G2 60-300 with image corrector. The FTIR spectra were obtained on a Nicolet 670 FT-IR spectrometer with KBr as the diluents. XPS data were obtained on Thermo ESCALAB250 instrument with a monochromatized Al Kα line source (200 W). Raman spectroscopic measurements were performed on a Renishaw in Via Raman System 1000 with a 532 nm Nd:YAG excitation source at room temperature. UV-vis DRS were performed on Varian Cary 500 Scan UV-visible system. Photoluminescence spectra were recorded on an Edinburgh FI/FSTCSPC 920 spectrophotometer. EPR measurements were performed using a Bruker model A300 spectrometer. Nitrogen adsorption-desorption isotherms were performed at 77 K using Micromeritics ASAP 2010 equipment. The concentration of Co^{2+} ions in water was recorded by monitoring the absorbance peak at 511 nm using a Varian Cary 50 UV-vis spectrophotometer. Photocurrent performance was conducted with a BAS Epsilon Electrochemical System in a conventional three electrode cell, using a Pt plate as the counter electrode and a saturated calomel electrode as the reference electrode.

Photocatalytic test

Reactions were experimented with a Pyrex top irradiation reactor connected to a glass closed gas-circulation system. Water photooxidation was carried out by dispersing the catalyst (50 mg) in 100 mL aqueous solution containing different amount of metal compounds. After stirring for 30 min, silver nitrate (0.17 g, as the electron acceptor) and La_2O_3 (0.2 g, as the pH buffer agent) were added. The reactant solution was evacuated several times to remove air completely before irradiation under a 300 W xenon lamp with an appropriate cut-off filter. The temperature of the solution was maintained at 12°C by a flow of cooling water during the reaction. The evolved gases were analyzed by a SHIMADZU GC-8A gas chromatograph with the thermal conductive detector, a 5 Å molecular sieve column and using argon as the carrier gas.

Received 1 November 2015; accepted 13 November 2015; published online 20 November 2015

1 Gratzel M. Photoelectrochemcial cells. Nature, 2001, 414: 338–344
2 Maeda K, Teramura K, Lu D, *et al.* Photocatalyst releasing hydrogen from water. Nature, 2006, 440: 295–295
3 Blankenship RE, Tiede DM, Barber J, *et al.* Comparing the efficiency of photosynthesis with photovoltaic devices and recognizing opportunities for improvement. Science, 2011, 332: 805–809
4 Hou Y, Abrams BL, Vesborg PCK, *et al.* Bioinspired molecular co-catalysts bonded to a silicon photocathode for solar hydrogen evolution. Nat Mater, 2011, 10: 434–438
5 Ma TY, Ran J, Dai S, Jaroniec M, Qiao SZ. Phosphorus-doped graphitic carbon nitrides grown *in situ* on carbon-fiber paper: flexible and reversible oxygen electrodes. Angew Chem Int Ed, 2015, 54: 4646–4650
6 Ran J, Zhang J, Yu J, Jaroniec M, Qiao SZ. Earth-abundant cocatalysts for semiconductor-based photocatalytic water splitting. Chem Soc Rev, 2014, 43: 7787–7812
7 Toma FM, Sartorel A, Iurlo M, *et al.* Efficient water oxidation at carbon nanotube-polyoxometalate electrocatalytic interfaces. Nat Chem, 2010, 2: 826–831
8 Duan L, Bozoglian F, Mandal S, *et al.* A molecular ruthenium catalyst withwater-oxidation activity comparable to that ofphotosystem II. Nat Chem, 2012, 4: 418–423
9 Kudo A, Miseki Y. Heterogeneous photocatalyst materials for water splitting. Chem Soc Rev, 2009, 38: 253–278.
10 Maeda K, Domen K. Photocatalytic water splitting: recent progress and future challenges. J Phys Chem Lett, 2010, 1: 2655–2661
11 Yeh TF, Syu JM, Cheng C, Chang TH, Teng H. Graphite oxide as a photocatalyst for hydrogen production from water. Adv Funct Mater, 2010, 20: 2255–2262
12 Qu Y, Zhong X, Li Y, *et al.* Photocatalytic properties of porous silicon nanowires. J Mater Chem, 2010, 20: 3590–3594
13 Wang F, Ng WKH, Yu JC, *et al.* Red phosphorus: an elemental photocatalyst for hydrogen formation from water. Appl Catal B, 2012, 111–112, 409–414
14 Liu G, Niu P, Yin L, Cheng HM. α-Sulfur crystals as a visible-light-active photocatalyst. J Am Chem Soc, 2012, 134: 9070–9073
15 Liu G, Yin YC, Niu P, Jiao W, Cheng HM. Visible-light-responsive beta-rhombohedral boron photocatalysts. Angew Chem Int Ed, 2013, 52: 6242–6245
16 Wang XC, Maeda K, Thomas A, *et al.* A metal-free polymeric photocatalyst for hydrogen production from water under visible light. Nat Mater, 2009, 8: 76–80
17 Liu J, Wen S, Hou Y, *et al.* Visible-light-responsive photocatalysts. Angew Chem Int Ed, 2013, 52: 3241–3245
18 Sprick RS, Jiang JX, Bonillo B, *et al.* Tunable organic photocatalysts for visible-light-driven hydrogen evolution. J Am Chem Soc, 2015, 137: 3265–3270
19 Ghosh S, Kouamé NA, Ramos L, *et al.* Conducting polymer nanostructures for photocatalysis under visible light. Nat Mater, 2015, 14: 505–511
20 Schwab MG, Hamburger M, Feng XL, *et al.* Photocatalytic hydrogen evolution through fully conjugated poly(azomethine) networks. Chem Commun, 2010, 46: 8932–8934
21 Novoselov KS, Geim AK, Morozov SV, *et al.* Electric field effect in atomically thin carbon films. Science, 2004, 306: 666–669

22 Aufray B, Kara A, Vizzini S, *et al.* Graphene-like silicon nanoribbons on Ag(110): a possible formation of silicone. Appl Phys Lett, 2010, 96: 183102
23 Song L, Liu Z, Reddy ALM, *et al.* Binary and ternary atomic layers built from carbon, boron, and nitrogen. Adv Mater, 2012, 24, 4878–4895
24 Hou YD, Laursen AB, Zhang JS, *et al.* Layered nanojunctions for hydrogen-evolution catalysis. Angew Chem Int Ed, 2013, 52: 3621–3625
25 Yang HG, Liu G, Qiao SZ, *et al.* Solvothermal synthesis and photoreactivity of anatase TiO_2 nanosheets with dominant {001} facets. J Am Chem Soc, 2009, 131: 4078–4083
26 Chhowalla M, Shin HS, Eda G, *et al.* The chemistry of two-dimensional layered transition metal dichalcogenide nanosheets. Nat Chem, 2013, 5: 263–275
27 Watanabe K, Taniguchi T, Kanda H. Direct-bandgap properties and evidence for ultraviolet lasing of hexagonal boron nitride single crystal. Nat Mater, 2004, 3: 404–409
28 Gong Y, Shi G, Zhang Z, *et al.* Direct chemical conversion of graphene to boron- and nitrogen- and carbon-containing atomic layers. Nat Commun, 2014, 5: 3193
29 Wang X, Zhi C, Li L, *et al.* "Chemical blowing" of thin-walled bubbles: high-throughput fabrication of large-area, few-layered BN and C_x-BN nanosheets. Adv Mater, 2011, 23: 4072–4076
30 Wang S, Zhang L, Xia Z, *et al.* BCN graphene as efficient metal-free electrocatalyst for the oxygen reduction reaction. Angew Chem Int Ed, 2012, 51: 4209–4212
31 Zhuang X, Mai Y, Wu D, Zhang F, Feng X. Two-dimensional soft nanomaterials: a fascinating world of materials. Adv Mater, 2015, 27: 403–427
32 Huang CJ, Chen C, Zhang MW, *et al.* Carbon-doped BN nanosheets for metal-free photoredox catalysis. Nat Commun, 2015, 6: 7698
33 Mazzoni MSC, Nunes RW, Azevedo S, Chacham H. Electronic structure and energetics of $B_xC_yN_z$ layered structures. Phys Rev B, 2006, 73: 073108
34 Watanabe MO, Itoh S, Sasaki T, Mizushima K. Visible-light-emitting layered BC_2N semiconductor. Phys Rev Lett, 1996, 77: 187–189
35 Lei W, Portehault D, Dimova R, Antonietti M. Boron carbon nitride nanostructures from salt melts: tunable water-soluble phosphors. J Am Chem Soc, 2011, 133: 7121–7127
36 Li J, Xiao X, Xu X, *et al.* Activated boron nitride as an effective adsorbent for metal ions and organic pollutants. Sci Rep, 2013, 3: 3208
37 Lei W, Portehault D, Liu D, Qin S, Chen Y. Porous boron nitride nanosheets for effective water cleaning. Nat Commun, 2013, 4: 1777
38 Wang SB, Ding ZX, Wang XC. A stable $ZnCo_2O_4$ cocatalyst for photocatalytic CO_2 reduction. Chem Commun, 2015, 51: 1517–1519
39 Chen S, Shen S, Liu G, *et al.* Interface engineering of a CoO_x/Ta_3N_5 photocatalyst for unprecedented water oxidation performance under visible-light-irradiation. Angew Chem Int Ed, 2015, 127: 3090–3094
40 Wang SB, Wang XC. Multifunctional metal-organic frameworks for photocatalysis. Small, 2015, 11: 3097–3112
41 Hyman MP, Vohs JM. Reaction of ethanol on oxidized and metallic cobalt surfaces. Surf Sci, 2011, 605: 383–389
42 Zhang JS, Grzelczak M, Hou YD, *et al.* Photocatalytic oxidation of water by polymeric carbon nitride nanohybrids made of sustainable elements. Chem Sci, 2012, 3: 443–446
43 Vakros J, Bourikas K, Perlepes S, Kordulis C, Lycourghiotis A. Adsorption of cobalt ions on the "electrolytic solution/γ-alumina" interface studied by diffuse reflectance spectroscopy (DRS). Langmuir, 2004, 20: 10542–10550
44 Zhang JS, Zhang MW, Sun RQ, Wang XC. A facile band alignment of polymeric carbon nitride semiconductors to construct isotype heterojunctions. Angew Chem Int Ed, 2012, 51: 10145–10149
45 Zhang GG, Huang CJ, Wang XC. Dispersing molecular cobalt in graphitic carbon nitride frameworks for photocatalytic water oxidation. Small, 2015, 11: 1215–1221
46 Zhang GG, Zang SH, Wang XC. Layered $Co(OH)_2$ deposited polymeric carbon nitrides for photocatalytic water oxidation. ACS Catal, 2015, 5: 941–947
47 Zhang GG, Zang SH, Lan ZA, *et al.* Cobalt selenide: a versatile cocatalyst for photocatalytic water oxidation with visible light. J Mater Chem A, 2015, 3: 17946–17950
48 Zheng Y, Lin LH, Wang B, Wang XC. Graphitic carbon nitride polymers toward sustainable photoredox catalysis. Angew Chem In Ed, 2015, 54: 12868–1288
49 Zhang JS, Chen Y, Wang XC. Two-dimensional covalent carbon nitride nanosheets: synthesis, functionalization, and applications. Energy Environ Sci, 2015, 8: 3092–3108

Acknowledgements This work was supported by the National Basic Research Program of China (2013CB632405) and the National Natural Science Foundation of China (21425309 and 21173043).

Author contributions The manuscript was written through contributions of all authors. All authors have given approval to the final version of the manuscript.

Conflict of interest The authors declare that they have no conflict of interest.

Supplementary information Supporting data are available in the online version of the paper.

Mingwen Zhang received his BSc degree in chemistry from Fuzhou University in 2011. He is currently a PhD candidate in physical chemistry under the supervision of Prof. Xinchen Wang at Fuzhou University. His current research is mainly focused on the development of novel nanostructure engineered photocatalysts for photocatalytic water splitting.

Xinchen Wang obtained his BSc degree from Fuzhou University and PhD degree from the Chinese University of Hong Kong. He was then a postdoctoral fellow at Tokyo University and an Alexander von Humboldt Fellow and a Group Leader at Max Planck Institute of Colloids and Interfaces, Germany. He is currently a professor at the State Key Laboratory of Photocatalysis on Energy and Environment, College of Chemistry, Fuzhou University, China. His research concerns designing solar energy materials for water splitting, CO_2 fixation, and organocatalysis with sunlight.

中文摘要 本文利用六方相硼氮碳(*h*-BCN)半导体光催化剂吸附钴离子, 构筑不含任何贵金属成分的光催化体系, 在可见光照射下, 实现水的催化氧化生成氧气反应. *h*-BCN半导体材料由于B–N离子键的"lop-sided"效应, 对金属离子具有很强的化学亲和性, 利用此性质并结合其高比表面积的特性, 制备出了一系列具有特殊性能的金属/*h*-BCN杂化层状结构. 研究结果表明, 在钴离子镶嵌的*h*-BCN(Co/*h*-BCN)杂化材料中, 金属和载体之间的协同作用能有效促进光生载流子分离、降低反应活化能, 进而提高光催化氧化水产氧性能. 本文展示了利用廉价和地球高丰度元素构筑不含贵金属成份的纳米层状复合材料, 有望将过渡金属催化和*h*-BCN光催化耦合, 实现面向可持续能源转换的协同催化过程.